doi:10.2533/chimia.2010.350 Chimia 64 (2010) 350–355

Molecular Electronics: Insight from First-Principles Transport Simulations

Magnus Paulsson[a], Thomas Frederiksen[b], and Mads Brandbyge*[c]

Abstract: Conduction properties of nanoscale contacts can be studied using first-principles simulations. Such calculations give insight into details behind the conductance that is not readily available in experiments. For example, we may learn how the bonding conditions of a molecule to the electrodes affect the electronic transport. Here we describe key computational ingredients and discuss these in relation to simulations for scanning tunneling microscopy (STM) experiments with C_{60} molecules where the experimental geometry is well characterized. We then show how molecular dynamics simulations may be combined with transport calculations to study more irregular situations, such as the evolution of a nanoscale contact with the mechanically controllable break-junction technique. Finally we discuss calculations of inelastic electron tunnelling spectroscopy as a characterization technique that reveals information about the atomic arrangement and transport channels.

Keywords: Density functional theory · Electron transport · Molecular dynamics · Molecular vibrations · Nanoscale contacts

Magnus Paulsson obtained his PhD in 2001 from Linköping University, Sweden. He is currently assistant professor at Linnaeus University, Sweden.

Thomas Frederiksen obtained his PhD in 2007 from the Technical University of Denmark. He is currently a postdoctoral fellow at the Donostia International Physics Center, Spain.

Mads Brandbyge obtained his PhD in 1997 from the Technical University of Denmark (DTU). He is associate professor at DTU, Department of Micro and Nanotechnology, Denmark.

1. Introduction

The vision of embedding electronic functions in single molecules is fascinating and both experimental and theoretical research in molecular electronics is rapidly advancing.[1–5] However, experiments are not straightforward to interpret since many details are unknown, *e.g.*, the role of the bonding to the electrodes and stability in the presence of current. In fact, current–voltage characteristics are typically the only direct pieces of information available from experiments. It is therefore important to be able to model the transport properties of molecular junctions in order to interpret and understand acquired data. The development of reliable simulation tools to predict the behaviour of molecular devices is further expected to be crucial for the development of new molecular-based electronics. It is desirable that this modelling is done with as few fitting parameters as possible.

In this paper we review how first-principles simulations can be used to investigate single-molecule contacts focusing on our previous work. We start with a description of the density functional nonequilibrium Green's function (DFT-NEGF) method and the concept of conduction eigenchannels. These channels give us a molecular orbital view of transport, here illustrated with recent simulations of scanning tunnelling microscopy (STM) contact experiments with C_{60} on Cu(111) surfaces. Since in this case the atomic details of both tip and surface electrodes are characterized prior to the contact experiment, it is possible to build an atomistic model that comes very close to reality. This allows for a detailed comparison of the conductance as a function of the tip–substrate separation. For other less-idealized contacts we proceed to show how molecular dynamics (MD) simulations combined with transport calculations can give insight into the role of contact geometries, the inter-electrode spacing, molecular conformations, and thermal motion of the atoms in the junction. Finally we discuss how inelastic electron spectroscopy yields fingerprints of the molecular structure in the current–voltage (*I-V*) characteristics.

2. The DFT-NEGF Method

Implementations of density functional theory (DFT) provide atomistic descriptions of total energy properties of nanosystems without system-specific adjustable parameters. In combination with the nonequilibrium Green's function (NEGF) method this has become a popular approach to calculate various aspects of electron transport in nanosystems.[6–11] The NEGF has made it possible to obtain the electronic structure, atomic forces, and transport in the presence of infinite electrodes, finite voltages, and currents. Standard equilibrium DFT of finite or periodic

*Correspondence: Dr. M. Brandbyge[c]
E-mail: Mads.Brandbyge@nanotech.dtu.dk
[a]School of Computer Science, Physics and Mathematics
Linnaeus University
391 82 Kalmar, Sweden
[b]Donostia International Physics Center (DIPC),
Manuel de Lardizabal
Pasealekua 4, 20018 Donostia, Spain
[c]Dept. of micro and nanotechnology (DTU-Nanotech)
Technical University of Denmark
2800 Kongens Lyngby, Denmark

systems offers an overall good description of chemical bonding and atomic structure. In contrast to other first-principles methods, DFT allows calculations on systems involving hundreds to thousands of atoms. Typical nanoscale transport systems are, due to the involvement of two or more electrodes connecting to the device, often at least of this size. Although DFT is targeting the total energy and not transport it is widely believed that DFT is a good starting point when it comes to balancing accuracy of method and system size. However, care must be exercised when using DFT for conductance calculations and comparison with benchmark experiments where the system is well-characterized is important. Below we show results obtained using the TranSIESTA method[7] which is now distributed with the SIESTA[12] pseudopotential density functional package. In addition to the TranSIESTA DFT-NEGF code, several other theory groups have during the last five years developed similar programs to perform DFT-NEGF calculations. Examples include Smegol,[9] gDFTB,[10] and one based on Turbomole.[11]

We will here consider molecular contacts bridging two semi-infinite metal electrodes. The result of the transport calculations on such systems is typically the total electron transmission $T_{tot}(E)$ through the contact structure as a function of energy E. The transmission is then related to the conductance *via* the Landauer-Büttiker formula. The transmission function is, in general, difficult to interpret and it is therefore useful to analyze the conduction in terms of transmission eigenchannels. Eigenchannels are particular electron scattering states starting from the left or right electrode with a well-defined transmission probability, $0 \leq T_i \leq 1$, where the individual eigenchannel transmissions add up to the total transmission $T_{tot} = \Sigma_i T_i$. As we will illustrate below, these channels can be viewed as resistors in parallel. Their corresponding scattering wavefunctions can be calculated with DFT-NEGF[13] and compared to the molecular orbitals of the contact in order to interpret the results.

The most important fact about the transmission eigenchannels is that the current for a molecular junction is typically carried by a few channels only. These channels thus yield a simpler basis for describing electron transport than the continuum of states originating from the electrodes. This is advantageous, *e.g.*, to analyze propensity rules for inelastic scattering against molecular vibrations.[14] The eigenchannel transmission coefficients have also been deduced in certain transport experiments[15,16] from measurements of the noise. Fig. 1 illustrates the concept of eigenchannel scattering states for a Au-wire as well as for two conjugated organic molecules [oligo-phenylene vinylene (OPV) and oligo-phenylene ethynylene (OPE)].[17] The calculated transmission at the Fermi level is close to unity for the Au-wire and significantly lower for the OPV ($T \approx 0.04$) and OPE ($T \approx 0.003$) junctions. In all cases >99.9% of the transmission is carried by the first eigenchannel. As seen in Fig. 1a the scattering state for the Au chain is a propagating state as expected for the highly transmitting channel. For the low-transmission OPV and OPE cases the scattering states rather resemble standing wave patterns.

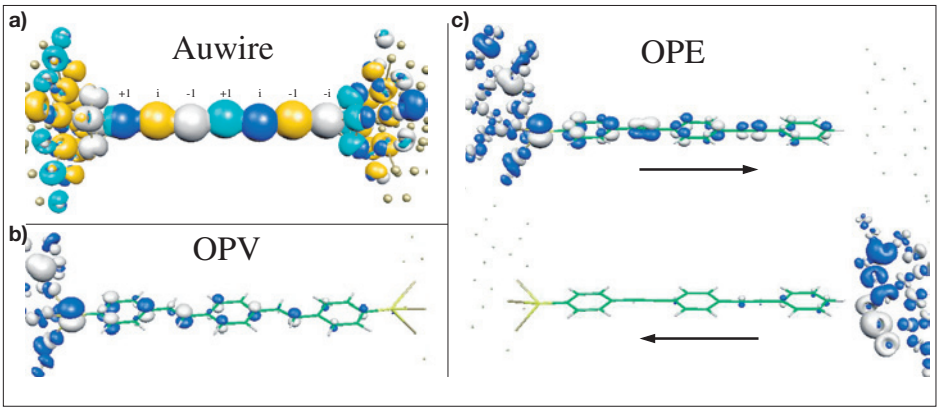

Fig. 1. (a) A propagating scattering state through a 7-atom Au-wire (incoming from left) is shown with the real (imaginary) part of the isosurface (with sign) in white/dark blue (orange/light blue). (b) Left eigenchannel scattering state (real part) for an OPV molecule thiol-bonded between two Au(111) surfaces. Because of the junction symmetry, the right eigenchannel (not shown) scattering state is essentially mirror symmetric to the left state. The colors correspond to the two different sign of the almost real-valued wavefunction (standing wave pattern). (c) Eigenchannel scattering states for an OPE molecule strongly bound by a thiol group to the left electrode and weakly interacting with the right electrode. Because of this asymmetric coupling the left and right scattering states (indicated by arrows) are considerably different. M. Paulsson, M. Brandbyge, *Phys. Rev. B* **2007**, *76*, 115117. Copyright 2007 American Physical Society.

In the OPV calculation the two thiol end-groups form covalent bonds to the hollow sites on the Au(111) surfaces. This allows – as seen in Fig. 1b – the conjugation of the molecule to continue through the sulfur atoms. For this symmetric junction the left and right eigenchannels are essentially mirror symmetric as expected. However, for asymmetric junctions the left and right scattering states for a given channel are qualitatively different. This is illustrated in Fig. 1c for the OPE molecule which is thiol-bonded to the left electrode but weakly coupled to the right electrode *via* the hydrogen termination.[13] Because of the tunnelling barrier at the interface to the right electrode the total transmission is more than an order of magnitude smaller than for the OPV junction. The asymmetry also has consequences for the current–voltage characteristics.[18]

3. Conductance of C_{60} Junctions

It is of interest to compare conductance calculations with the DFT-NEGF method to experiments where the junction geometry is known to a large extent. In recent STM experiments[19,20] it was possible to infer the orientation and adsorption site of a C_{60} on a Cu metal surface and subsequently make contact to the molecule using the tip. Besides the single C_{60} contact it was furthermore possible to transfer a C_{60} to the tip-electrode and thus use this functionalized tip to make contact to flat, clean Cu(111) surfaces as well as other C_{60} molecules, thereby also forming a C_{60}-C_{60} molecular wire. These three distinct cases are illustrated in Fig. 2a. The main uncertainties in these experiments are the tip structure and the absolute distances between tip and sample. These important factors can be inferred from a comparison with DFT-NEGF calculations as we will proceed to explain.

For a transparent interpretation of the experimental results the tip–molecule separation was considered the only variable in the simulation, and full geometry relaxations were not performed.[19] Except for the structural rearrangements expected with a sharp metallic tip (case 1),[20] this approach reproduces and explains the observed traces. The calculated conductances (Fig. 2b) enable a calibration of the absolute tip–molecule distance z (Cu to C_{60}-center along the surface normal) by aligning the tunnelling part of the traces. Comparison of cases 1 and 2 shows that for a given distance z, depending on the geometry of the molecule–electrode interface, the conductance of a single C_{60} junction can vary by a factor of 3 (10) under contact (tunnelling) conditions. The conductance of the C_{60}/Cu(111) junctions is dominated by the molecular LUMO resonances that lie closest to the Fermi energy. The theoretical maximum is therefore

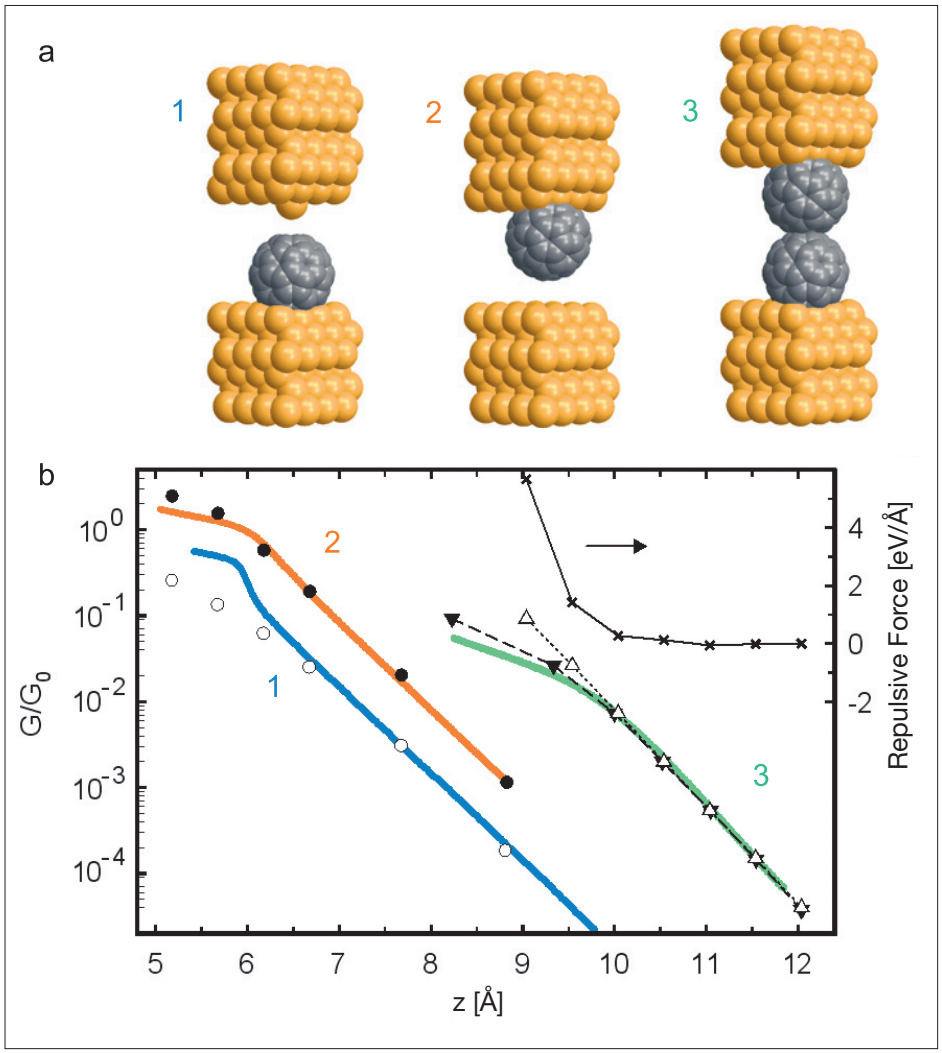

Fig. 2. (a) Sketches of the contact experiments performed by approaching (1) a sharp metallic tip to a C_{60} adsorbed on a hexagon on Cu(111), (2) a 5:6 oriented C_{60} tip to the bare Cu(111) surface, (3) a 5:6 oriented C_{60} tip to a C_{60} adsorbed on a hexagon on Cu(111). (b) Experimental (full lines) and calculated (symbols) conductances of the junctions versus the tip-molecule distance (1 and 2) and the C_{60} to C_{60} center distance (3). The calculated strong repulsive force between two C_{60} molecules (crosses) at small separations suggests an elastic deformation of the junction that maps real molecule-molecule distances (open triangles) with apparent distances (filled triangles), see text. G. Schull, T. Frederiksen, M. Brandbyge, R. Berndt, *Phys. Rev. Lett.* **2009**, *103*, 206803. Copyright 2009 American Physical Society.

3 G_0(= 2 e^2/h, e is the electron charge and h is Planck's constant), corresponding to a symmetric junction with resonant transport *via* the threefold degenerate LUMO states of the free C_{60}. Indeed, a decomposition of the conductance into eigenchannel contributions confirms that the three most transmitting channels carry about an order of magnitude more current than the fourth. For the sharp-tip contact (case 1) the eigenchannel transmissions in contact are of the order $T_i \approx \{0.12,0.08,0.04,0.004\}$, hence the majority of an incoming electron wave is being reflected in this type of junction. In contrast, for the C_{60}–tip contact (case 2 in Fig. 2a) three channels are much more open, theoretically in one case as much as $T_i \approx \{0.97,0.87,0.57,0.02\}$.[19]

The ability to visualize eigenchannels can next be used to analyze *where* the electrons are being scattered (Fig. 3a). In case 1 (sharp tip) the current is scattered at the single-atom contact to the molecule. In case 2 (C_{60}–tip) the channel is almost perfectly open and the scattering state is a propagating wave with essentially equal weight on either side of the molecule. The multiple atomic contact in case 2 thus ensures a better connection between molecule and electrode. This characterization of the metal–molecule contact could be valuable for fullerene-based anchoring strategies for molecular electronics.[21] In the case of C_{60}–C_{60} contacts the conductance ist suppressed by about a factor of 10 compared to the single C_{60} contacts, and is reaching maximum conductance in the region of significant intermolecular repulsion and elastic deformation (Fig. 2b, curve 3). The lower conductance is reminiscent of the semi-conducting gap appearing in the transmission for longer chains of C_{60} corresponding to a decaying wavefunction along the chain (Fig. 3, case 4). In summary, contrary to most transport experiments where the precise knowledge of the structure is very limited, these measurements on different C_{60} contacts are exceptional because the conformation of the junction and bonding to the electrodes are known from the start. The excellent agreement between experimental and theoretical conductance traces thus enables a complete characterization of the contacts.

4. Molecular Dynamics

Many transport measurements are performed using mechanically controllable break junctions without the possibility to determine the structure of the contacts formed. The evolution of the conductance is typically monitored as many contacts are broken, followed by a statistical analysis[22] of the conductance distribution. For these experiments it is of interest to theoretically investigate the possible scenarios for the evolution of geometry and conductance during the opening and closing processes. Such studies can give insight into the role played by contact chemistry and molecular conformation on the transport. Here we illustrate our studies starting from a gold point contact with the alkanedithiol molecule (Au-S-C_8H_{16}-S-Au) attached to the two metallic leads (Fig. 4) and investigate the stretching of the junction using MD simulations.[23] The stretching of the junction was performed at 300 K and a stretching speed of 170 m/s. It is important to note that due to the long computation times, it is inevitable to use stretching speeds many orders of magnitude larger than in any experiment. The MD simulations thus sample a smaller part of the geometrical phase space which in turn is likely to over-emphasize local energy minima configurations. Highly elongated structures are, in our opinion, especially prone to this effect because on the time scale of the experiments such metastable structures are likely to either break or pull out additional gold atoms. Although we sample a small part of the phase space, MD simulations are a convenient way to investigate many conformations that are all possible in the experiments.

The formation of one of the octanedithiol junctions is seen in Fig. 4. The simulation shows the breaking of the gold point contact (after about 3–4 Å of stretch), a straightening of the molecule (4–7 Å), migration of the thiol end-groups (7–14 Å), and pulling out of gold atoms from the surface (14–18 Å)[24,25] before the junction breaks at a gold–sulphur bond (19

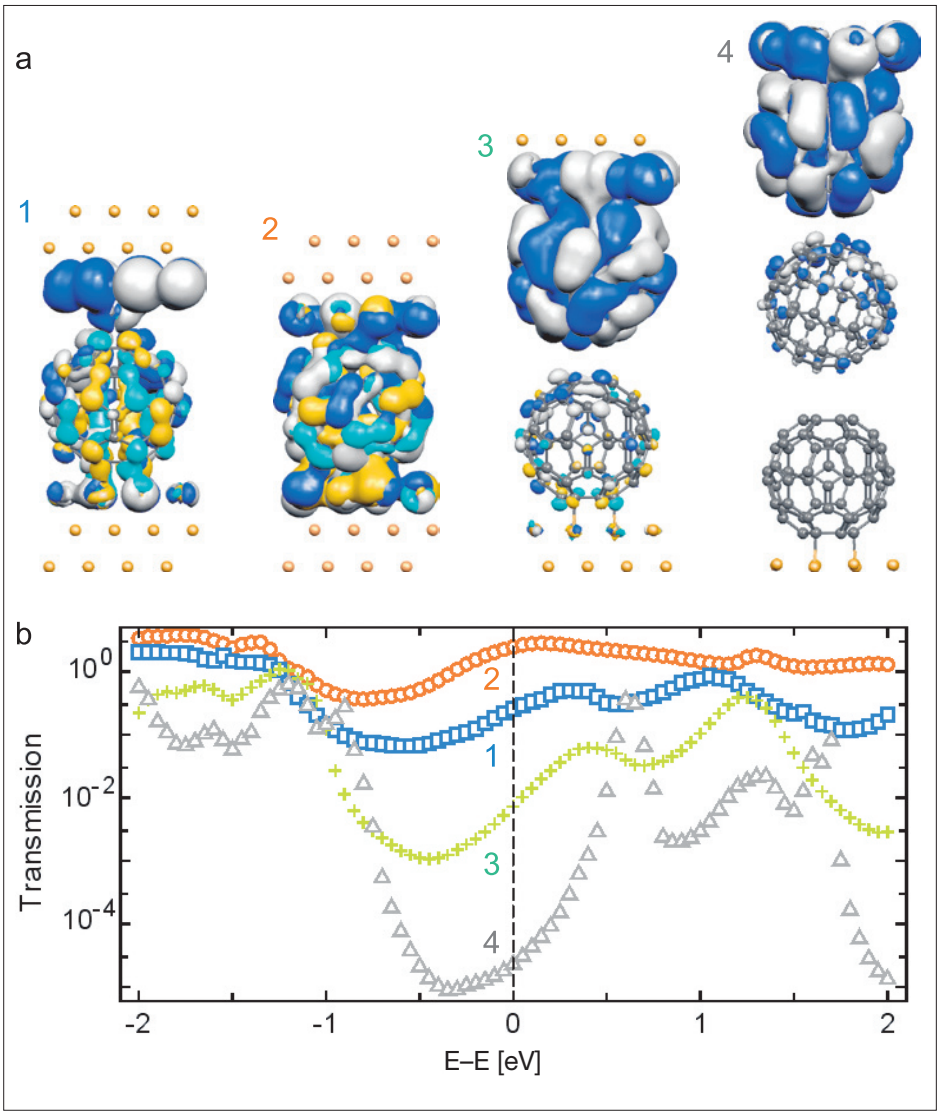

Fig. 3. (a) Visualizations of the most transmitting eigenchannels scattering states (incoming from above). The isosurfaces show the real (imaginary) part of the wave functions (with sign) in white/dark blue (orange/light blue). (b) Calculated transmission functions for suspended molecular chains made of one, two, or three C_{60} molecules. The molecular orientations correspond to (1) an adatom vs. a hexagon, (2) a 5:6 bond vs. a flat surface, (3) a hexagon vs. a 5:6 bond, and (4) a hexagon vs. a 5:6 bond vs. a hexagon. G. Schull, T. Frederiksen, M. Brandbyge, R. Berndt, *Phys. Rev. Lett.* **2009**, *103*, 206803. Copyright 2009 American Physical Society.

Å). During the initial phase the transmission shows a plateau around unity corresponding to an atomic gold point contact. When this contact breaks the transmission rapidly drops to ~10^{-4} with large fluctuations as a function of time. We have verified that these fluctuations are thermal fluctuations by continuing the MD simulations at different temperatures without stretching. However, as the time-scale of the conductance fluctuations is femtosecond, measurements will average these out. To correlate the transmission with the conformation of the alkane chain we show the evolution of dihedral angles and the number of the thiol–Au bonds, see Fig. 4. Surprisingly, the details of the thiol–Au bonds have limited influence on the transmission through the molecule. However, from the MD simulations we found several examples where gauche defects lower the transmission by approximately an order of magnitude. One example of a gauche defect can be seen in Fig. 4 around 5.0–7.0 Å stretch, where the 'twist' of the alkane chain is clearly visible. Although the low-bias conductance values in these calculations are in reasonable agreement with experiments on octanedithiols[23] it is still difficult to conclude on the geometries in the experiments.

Fig. 4. (left) Snapshots of the formation of an octanedithiol molecular junction simulated using DFT-based molecular dynamics. As the junction is being stretched, the molecule migrates into the junction and pulls out a short gold chain before finally breaking. (right) Calculated electron transmission probability as a function of stretching distance. The number of Au–S bonds (defined by $r_{Au\text{-}S}$<3.3 Å) and dihedral angles for the S-C_8-S chain are also shown. M. Paulsson, C. Krag, T. Frederiksen, M. Brandbyge, *Nano Lett.* **2009**, *9*, 117. Copyright 2009 American Chemical Society.

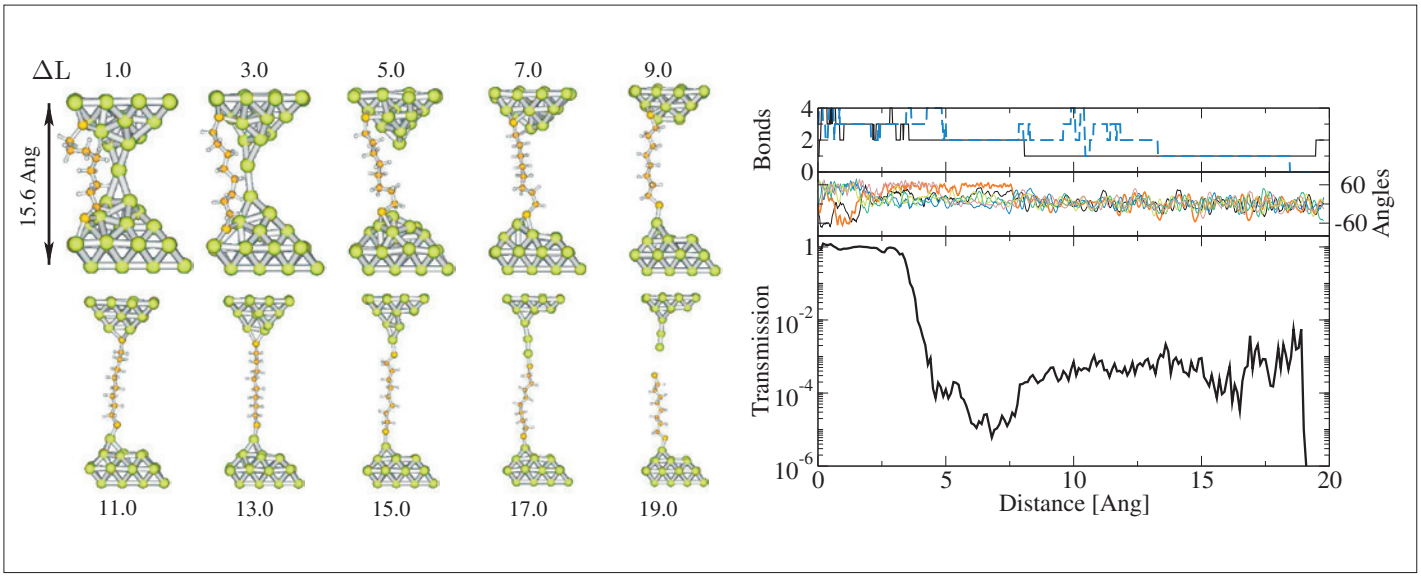

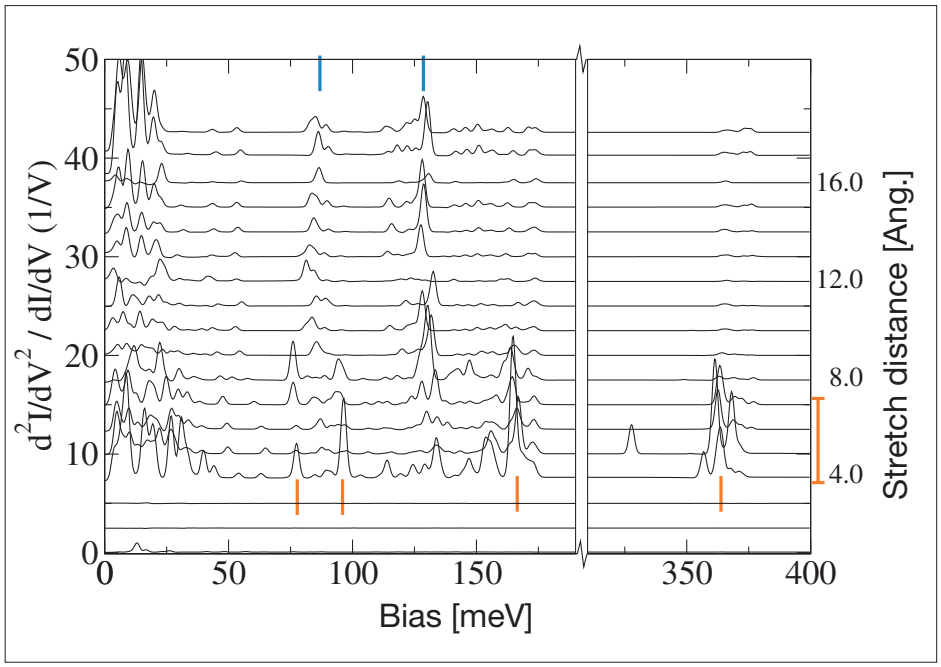

Fig. 5. Calculated inelastic electron tunneling spectra with the different stretching distances offset by 2.5 V^{-1}. The geometries with gauche defects are marked in the right margin for stretching 4.0–7.0 Å. Highlighted frequency bands are (i) top, ~82 (degenerate C–S) and 130 (C–C) meV, and (ii) bottom, 75 (non-degenerate C–S closest to defect), 95 (rock), 165 (wag) and 365 (C–H close to defect) meV. M. Paulsson, C. Krag, T. Frederiksen, M. Brandbyge, *Nano Lett.* **2009**, *9*, 117. Copyright 2009 American Chemical Society.

5. Scattering by Vibrations

Up to this point we have focused on the low-bias conductance of molecular junctions. Since this is only a single quantity characterizing the contact it is desirable to obtain more information from additional measurements. Suggestions include i) studies of the thermoelectric effect which can provide information on the position of the molecular resonances,[26–28] ii) measurements on gated molecular structures[5] to determine the conductance variation with a gate voltage, and iii) measurements of inelastic scattering against molecular vibrations to extract information about localized vibrations in the contact.[16] The latter technique, called inelastic electron tunnelling spectroscopy (IETS), has so far been the most successful way to characterize nanoscale contacts.

IETS is a spectroscopic technique that measures the changes in conductance associated with phonon (vibration) emission at low temperatures. An intuitive understanding of the IETS can be reached from the Fermi golden rule, where an initial electron state is scattered by emission of a phonon to a lower-energy final state. Since the Pauli principle block scattering into filled final states, the bias has to exceed the vibrational energy for the transition to occur. This implies that the conductance will contain small corrections at bias thresholds matching the vibrational energies. However, due to noise, experimentalists often measure the second derivative of the current–voltage characteristics directly with the lock-in technique and thereby observe peaks or dips at the threshold voltages. The IETS technique has been used i) to verify that a molecule of interest is present in the junction[29] and ii) to learn more about the detailed geometric structure.[30,31]

The calculation of IETS signals is considerably more complicated compared to the elastic transmission calculations. However, we have developed computationally efficient approximations to calculate the inelastic corrections to the current–voltage characteristics.[30,32] Using a finite difference method coupled to the SIESTA DFT code, we calculate the electron–phonon coupling and vibrational frequencies without parameters and use this in conjunction with TranSIESTA calculations to obtain the IETS fully from first principles. Our implementation scheme has been dubbed Inelastica.[33] To illustrate the IETS calculations we show the calculated IETS for the MD simulation in Fig. 4. The calculations are performed by taking the MD geometry for each 1 Å stretch.

The resulting IETS are shown in Fig. 5 for each stretch 1.0–18.0 Å. We note that the main IETS signals seen in experiments[29,34–37] and in numerical calculations[17,38,39] are present here, *e.g.*, C–C (~130 meV), C-S (82 meV), C-H (365 meV), rock (95 meV), and wag (165 meV). The stretching distances, marked in the right margin of Fig. 5, that correspond to geometries containing the gauche defect are those between 4.0–7.0 Å. Note the qualitative different IETS with and without the defect. This illustrates that the IETS is sensitive to details of the molecular junction conformation. It is thus possible to obtain a wealth of information from the IETS not available in other transport experiments. Future research on the IETS thus promises an increased understanding of transport in molecular junctions and enables us to critically compare theory to experiments.

6. Summary and Outlook

Calculation techniques for electron transport through molecular junctions have advanced significantly during the last ten years. Today several software packages provide the possibility to use density functional theory combined with nonequilibrium Green's function techniques to calculate current–voltage characteristics including a voltage drop across the molecule. We have exemplified these advances with calculations on C_{60} contacts and molecular dynamics simulations of alkanedithiol molecules. These methods are now mature to address thermoelectric effects and inelastic electron tunnelling spectroscopy.

The field of molecular electronics is currently driven by increasingly advanced experimental methods aiming to reliable build and characterize high quality molecular junctions with well-defined contacts to the molecule. This allows for critical comparison between theory and experiment. Theoretical modelling of transport in molecular junctions can further be expected to play a key role for design and optimization of future applications of molecular nanostructures.

Received: April 20, 2010

[1] C. Joachim, J. K. Gimzewski, A. Aviram, *Nature* **2000**, *408*, 541.
[2] A. Nitzan, M. A. Ratner, *Science* **2003**, *300*, 1384.
[3] S. Wu, M. T. González, R. Huber, S. Grunder, M. Mayor, C. Schönenberger, M. Calame, *Nat. Nanotechnol.* **2008**, *3*, 569.
[4] K. Moth-Poulsen, T. Bjørnholm, *Nat. Nanotechnol.* **2009**, *4*, 551.
[5] H. Song, Y. Kim, Y. H. Jang, H. Jeong, M. A. Reed, T. Lee, *Nature* **2009**, *462*, 1039.
[6] J. Taylor, H. Guo, J. Wang, *Phys. Rev. B* **2001**, *63*, 245407.
[7] M. Brandbyge, J. L. Mozos, P. Ordejón, J. Taylor, K. Stokbro, *Phys. Rev. B* **2002**, *65*, 165401.
[8] A. Pechia, A. Di Carlo, *Rep. Prog. Phys.* **2004**, *67*, 1497.
[9] A. R. Rocha, V. M. García-Suárez, S. W. Bailey, C. J. Lambert, J. Ferrer, S. Sanvito, *Nat. Mater.* **2005**, *4*, 335.
[10] J. R. Reimers, G. C. Solomon, A. Gagliardi, A. Bilic, N. S. Hush, T. Frauenheim, A. Di Carlo, A. Pechia, *J. Phys. Chem. A* **2007**, *111*, 5692.

[11] F. Pauly, J. K. Viljas, U. Huniar, M. Häfner, S. Wohlthat, M. Bürkle, J. C. Cuevas, G. Schön, *New J. Phys.* **2008**, *10*, 125019.
[12] J. M. Soler, E. Artacho, J. D. Gale, A. García, J. Junquera, P. Ordejón, D. Sánchez-Portal, *J. Phys.: Condens. Matter* **2002**, *14*, 2745.
[13] M. Paulsson, M. Brandbyge, *Phys. Rev. B* **2007**, *76*, 115117.
[14] M. Paulsson, T. Frederiksen, H. Ueba, N. Lorente, M. Brandbyge, *Phys. Rev. Lett.* **2008**, *100*, 226604.
[15] E. Scheer, N. Agraït, J. C. Cuevas, A. L. Yeyati, B. Ludoph, A. Martin-Rodero, G. Rubio-Bollinger, J. M. van Ruitenbeek, C. Urbina, *Nature* **1998**, *394*, 154.
[16] N. Agraït, A. L. Yeyati, J. M. van Ruitenbeek, *Phys. Rep.* **2003**, *377*, 81.
[17] M. Paulsson, T. Frederiksen, M. Brandbyge, *Nano Lett.* **2006**, *6*, 258.
[18] J. Taylor, M. Brandbyge, K. Stokbro, *Phys. Rev. Lett.* **2002**, *89*, 138301.
[19] G. Schull, T. Frederiksen, M. Brandbyge, R. Berndt, *Phys. Rev. Lett.* **2009**, *103*, 206803.
[20] N. Néel, J. Kröger, L. Limot, T. Frederiksen, M. Brandbyge, R. Berndt, *Phys. Rev. Lett.* **2007**, *98*, 065502.
[21] C. A. Martin, D. Ding, J. K. Sørensen, T. Bjørnholm, J. M. van Ruitenbeek, H. S. J. van der Zant, *J. Am. Chem. Soc.* **2008**, *130*, 13198.
[22] M. T. González, J. Brunner, R. Huber, S. Wu, C. Schönenberger, M. Calame, *New J. Phys.* **2008**, *10*, 065018.
[23] M. Paulsson, C. Krag, T. Frederiksen, M. Brandbyge, *Nano Lett.* **2009**, *9*, 117.
[24] R. J. C. Batista, P. Ordejon, H. Chacham, E. Artacho, *Phys. Rev. B* **2007**, *75*, 041402.
[25] E. Anglada, J. A. Torres, F. Yndurain, J. M. Soler, *Phys. Rev. Lett.* **2007**, *98*, 096102.
[26] M. Paulsson, S. Datta, *Phys. Rev. B* **2003**, *67*, 241403.
[27] P. Reddy, S.-Y. Jang, R. A. Segalman, A. Majumdar, *Science* **2007**, *315*, 1568.
[28] A. Tan, S. Sadat, P. Reddy, *Appl. Phys. Lett.* **2010**, *96*, 13110.
[29] C. R. Arroyo, T. Frederiksen, G. Rubio-Bollinger, M. Velez, A. Arnau, D. Sanchez-Portal, N. Agraït, *Phys. Rev. B* **2010**, *81*, 075405.
[30] T. Frederiksen, M. Paulsson, M. Brandbyge, A. P. Jauho, *Phys. Rev. B* **2007**, *75*, 205413.
[31] M. Galperin, M. A. Ratner, A. Nitzan, A. Troisi, *Science* **2008**, *319*, 1056.
[32] M. Paulsson, T. Frederiksen, M. Brandbyge, *Phys. Rev. B* **2005**, *72*, 201101.
[33] The Inelastica code is freely available for download at *http://sourceforge.net/projects/inelastica/*.
[34] D. P. Long, J. L. Lazorcik, B. A. Mantooth, M. H. Moore, M. A. Ratner, A. Troisi, Y. Yao, J. W. Ciszek, J. M. Tour, R. Shashidhar, *Nat. Mater.* **2006**, *5*, 901.
[35] J. M. Beebe, H. J. Moore, T. R. Lee, J. G. Kushmerick, *Nano Lett.* **2007**, *7*, 1364.
[36] N. Okabayashi, Y. Konda, T. Komeda, *Phys. Rev. Lett.* **2008**, *100*, 217801.
[37] N. Okabayashi, M. Paulsson, H. Ueba, Y. Konda, T. Komeda, *Phys. Rev. Lett.* **2010**, *104*, 077801.
[38] G. C. Solomon, A. Gagliardi, A. Pechia, T. Frauenheim, A. Di Carlo, J. R. Reimers, N. S. Hush, *J. Chem. Phys.* **2006**, *124,* 094704.
[39] D. P. Long, A. Troisi, *A. J. Am. Chem. Soc.* **2007**, *129*, 15303.